NMR IN BIOMEDICINE
NMR Biomed. 2001;**14**:77–93
DOI:10.1002/nbm.682

Review Article

The effects of microscopic tissue parameters on the diffusion weighted magnetic resonance imaging experiment

David G. Norris*

Max-Planck-Institute of Cognitive Neuroscience, Leipzig, Germany

Received 10 February 2000; revised 18 October 2000; accepted 25 October 2000

ABSTRACT: This review examines the way in which microscopic tissue parameters can affect MR experiments which are sensitive to diffusion. The interaction between the intra- and extravascular as well as that between the intra- and extracellular spaces is examined. Susceptibility gradients due to the presence of deoxyhemoglobin can cause diffusion-induced signal losses which are significant in functional magnetic resonance experiments, particularly at higher main magnetic field strengths. This is also true of the fast response that manifests itself as an early negative signal change in functional magnetic resonance experiments. The fields surrounding paramagnetic vessels are described and the way in which diffusion in these fields contributes to functional signal changes is examined. Flow in the capillary bed can be a confounding factor in experiments which aim to examine the diffusion characteristics of extravascular water. It is potentially also a method for assessing capillary perfusion. The intravoxel incoherent motion experiment is described in terms of how significantly this effect can influence diffusion attenuation curves from water. The major models for describing water diffusion in tissue are presented, as are the main experimental results that have contributed to an understanding of the mechanisms of diffusion contrast. The widely accepted view that changes in the diffusion characteristics are caused by a shift of water to the intracellular space and a concomitant change in extracellular tortuosity is examined critically. More recent experiments that indicate that a reduction in the intracellular diffusion may occur simultaneously with the cell swelling are described and their compatibility with existing models discussed. Copyright © 2001 John Wiley & Sons, Ltd.

KEYWORDS: magnetic resonance imaging; diffusion imaging; perfusion imaging; functional magnetic resonance; ischemia; diffusion anisotropy; mechanisms of diffusion contrast

INTRODUCTION

During the early development of MRI, diffusion did not play a significant role: the first experiments combining diffusion weighting with imaging were not published until 1984[1] and the first from a whole-body system appeared in 1986.[2] Historically, it is of note that some of the earliest NMR experiments were significantly affected by diffusion within the liquid sample caused by the presence of inhomogeneity gradients.[3,4] Indeed the well-known Carr–Purcell sequence[4] was developed in order to separate the effects of diffusion and T_2 relaxation.

Since the early 1990s diffusion-weighted imaging (DWI) has assumed an important role both in clinical routine and in the research environment.[5–8] Despite numerous technical difficulties associated with bulk motion[9–11] and eddy currents,[12–15] combined with the high demands placed on the gradient system, DWI is in widespread use because of its exquisite sensitivity to changes in the displacement characteristics of water molecules. The primary application for this methodology is in the early detection of cerebral ischemia,[5–8] although the advent of diffusion tensor imaging (DTI)[16–20] has also made it possible to image the fiber tracts in white matter of the brain and potentially in other organs such as the heart.[21] Furthermore, diffusion-weighted imaging is potentially sensitive to flow in the capillary system,[22]

**Correspondence to:* D. G. Norris, Max-Planck-Institute of Cognitive Neuroscience, Stephanstr. 1a, D-04103 Leipzig, Germany.
E-mail: norris@cns.mpg.de

Abbreviations used: 2FDG-6P, 2-fluoro-2-deoxyglucose-6-phosphate; ADC, apparent diffusion coefficient; BOLD, blood oxygen level dependent; CNS, central nervous system; CSF, cerebro spinal fluid; DTI, diffusion tensor imaging; DWI, diffusion weighted imaging; fMR, functional magnetic resonance; FR, fast response; IVCM, intravoxel coherent motion; IVIM, intravoxel incoherent motion; MCAO, middle cerebral artery occlusion; MRI, magnetic resonance imaging; NMDA, *N*-methyl-D-aspartate; NMR, nuclear magnetic resonance; PFG, pulsed field gradient; rBF, regional blood flow; SGP, short gradient pulse; *TE*, echo time.

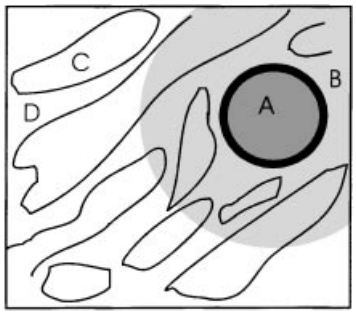

Figure 1. The cell structure shown schematically in anisotropic tissue and a blood capillary. Region A is within the capillary and a region of modified magnetic field caused by paramagnetic deoxyhemoglobin within the capillary is denoted by the shaded area (B) which surrounds it. The intracellular compartment is given by C, and the extracellular by D

and a significant component of the signal intensity changes in functional magnetic resonance imaging of the brain arises from diffusion effects.[23]

It is thus clear that diffusion is of central importance to modern methods of imaging, particularly for the central nervous system (CNS). In this review article the effects of microscopic tissue structure on the diffusion of water will be examined, with an emphasis on imaging the CNS, although some of the results are also applicable to other tissues. The essential physiology that will be examined consists of the intra- and extravascular spaces, with the latter being further divided into the intra- and extracellular spaces. These are shown schematically in Fig. 1. Water exchanges freely between these spaces, which are considered to be separated by semi-permeable barriers.[24,25] In healthy brain tissue the intravascular compartment occupies about 3–4% by volume with the remainder divided in the ratio of 4:1 between the intra- and extracellular spaces. The emphasis is on how diffusion can affect the results of MR imaging experiments, irrespective as to whether the experiment is deliberately diffusion sensitized.

The structure of the article is that after this Introduction is a short section (General Theory) describing the basic mathematics of diffusion as applicable to MRI. There are then two major sections: First the interaction between the intra- and extravascular spaces is examined, and then that between the intra- and extracellular spaces.

GENERAL THEORY

In this section a short summary of the standard theory pertaining to diffusion in NMR experiments is given, for a more detailed treatment the reader is advised to consult one of the numerous specialist texts on this subject.[26,27]

The NMR experiment in the presence of isotropic diffusion is described by the modified Bloch equations[28]

$$\frac{\partial \mathbf{M}_{xy}(\mathbf{r},t)}{\partial t} = i\gamma \mathbf{G}\cdot\mathbf{r}\mathbf{M}_{xy}(\mathbf{r},t) + D\nabla^2\mathbf{M}_{xy}(\mathbf{r},t) \quad (1)$$

where $\mathbf{G}$ is the magnetic field gradient vector, D the diffusion coefficient, and $\mathbf{M}_{xy}$ is the transverse magnetisation at time t, and position vector $\mathbf{r}$. For unrestricted diffusion it is possible to solve these equations for arbitrary time courses of the gradient fields. In one of the simplest cases, a constant gradient applied during a spin-echo experiment, the solution is

$$\mathbf{M}_{xy}(\mathbf{r},t) = \mathbf{M}_{xy}(\mathbf{r},t=0)\exp(-2\gamma^2|\mathbf{G}|^2 D\tau^3/3) \quad (2)$$

where the echo time, TE is equal to 2τ. This shows that the signal attenuation caused by free diffusion is governed by an exponential decay with the attenuation coefficient proportional to the square of the magnetic field gradient strength and to the cube of the time of application of the gradient. This equation is also pertinent to constant susceptibility gradients, and illustrates that diffusion effects may undergo a rapid transition from being negligible, to having a significant effect on the signal intensity.

The standard methodology employed in most DWI experiments is the Stejskal and Tanner or pulsed field gradient (PFG) sequence.[29] In this two magnetic field gradient pulses of strength $\mathbf{G}$ and duration δ with a temporal separation of Δ between the onset of the pulses are applied. The attenuation of the MR signal due to diffusion is then given by

$$\mathbf{M}_{xy}(\mathbf{r},t) = \mathbf{M}_{xy}(\mathbf{r},t=0)\exp\left[-D(\gamma|\mathbf{G}|\delta)^2\left(\Delta-\frac{\delta}{3}\right)\right] \quad (3)$$

where the b-factor is defined as

$$b = (\gamma|\mathbf{G}|\delta)^2\left(\Delta-\frac{\delta}{3}\right) \quad (4)$$

It is common practice to define the parameter $\mathbf{q}$ as

$$2\pi\mathbf{q} = \gamma\mathbf{G}\delta \quad (5)$$

If the effects of diffusion during the gradient pulses in the PFG experiment can be neglected (this is generally known as the short gradient pulse, or SGP approximation) then $\mathbf{q}$ defines an inverse displacement space in analogy to the $\mathbf{k}$-vector which defines a k-space which is the inverse of position. However the use of $\mathbf{q}$ as a parameter is common even when the SGP approximation is not fulfilled.

In experiments in which diffusion is unrestricted the PFG experiment gives a mono-exponential dependence of the signal attenuation on the diffusion weighting. This is also true for many *in vivo* experiments. Concern regarding the effect of coherent flow in the vasculature on the diffusion weighted experiment lead to the term

'apparent diffusion coefficient' (ADC) to describe the *in vivo* diffusion coefficient.[2]

Diffusion may be restricted by impermeable barriers, or hindered by permeable ones. The mean square displacement determines the degree to which the diffusing molecules impinge on these barriers. According to the Einstein relation the expectation value of the mean square displacement for free diffusion in three dimensions ($\langle \mathbf{r}^2 \rangle$) is related to the diffusion coefficient and the diffusion time (τ_D) by

$$\langle \mathbf{r}^2 \rangle = 6D\tau_D \tag{6}$$

For an MR experiment the diffusion time is clearly related to the time for which the spins are allowed to diffuse in the presence of the diffusion-weighting gradients, and is hence a parameter which may be varied within the limits pertaining to a particular experiment. For the PFG experiment the signal attenuation as given by eqn (3) is proportional to $\langle \mathbf{r}^2 \rangle$ for a reduced diffusion time given by

$$\tau_D = \Delta - \delta/3 \tag{7}$$

A decrease in the diffusion coefficient as a function of increasing diffusion time may hence be interpreted as an indication of restricted diffusion.

THE INTERACTION OF THE INTRA- AND EXTRAVASCULAR SPACES

This section is concerned with two effects. The first is that the presence of deoxyhemoglobin in the vasculature generates susceptibility gradients which will generally extend into the extravascular space. This is of significance in functional magnetic resonance investigations, where changes in deoxyhemoglobin concentration as a result of functional activation will modify the susceptibility gradients about blood vessels, and consequently the diffusion attenuation in these gradients. The second effect is due to coherent flow in the intravascular compartment, which here dominates over diffusion, because for typical diffusion times the molecular displacement caused by flow will be much greater than that caused by diffusion. This is hence not only a possible confounding factor for diffusion weighted experiments, but also potentially offers a means of detecting capillary perfusion.

Functional Magnetic Resonance (fMR)

Since its discovery, fMR[30,31] has developed into a major tool in experimental psychological research and neurological research, as well as finding clinical applications. It is not intended here to discuss fMR as such, which is beyond the scope of this article, but to describe how diffusion effects are fundamental to fMR contrast.

The chain of events that occurs in response to increased neuronal activity can be concisely described as follows: the increased activity results in an increased rate of metabolic oxygen consumption, and hence in an increased concentration of deoxyhemoglobin. In order to satisfy this increased requirement for oxyhemoglobin the blood flow subsequently increases locally to such an extent that the deoxyhemoglobin concentration is reduced in comparison with the resting state. This leads to a relative decrease in signal during the initial phase where the deoxyhemoglobin concentration is increased, which is often known as the fast response (FR),[32] and a subsequent increase in signal during the period of increased rBF. This contrast is generically known as BOLD[33,34] (blood oxygen level dependent) and results both from static dephasing of the signal due to local shifts in the resonance frequency, and from diffusion-related losses. If we consider blood vessels as being infinitely long paramagnetic cylinders then the field distribution about the vessel will be given by[23]

$$\Delta\omega(r,\theta,\phi) = K \sin^2\theta \cos(2\phi) \left(\frac{a}{r}\right)^2 \tag{8}$$

with

$$K = 2\pi\omega_0 \Delta\chi (1 - Y) \tag{9}$$

where θ is the angle between the long axis of the vessel and the main magnetic field, r is the radial coordinate in a plane perpendicular to the vessel, ϕ is the angular coordinate within this plane with $\phi = 0$ defined by the projection of the main magnetic field onto the plane. $\Delta\chi$ is the volume susceptibility difference between blood in the vessel and the surroundings, Y is the fractional degree of blood oxygenation and a is the vessel radius. This equation indicates that the magnetic field generated by the presence of a paramagnetic cylinder is dependent on its orientation: if it is parallel to the direction of the static field then no additional field will be generated. The field has its greatest value if the axis of the cylinder is perpendicular to the main field. The spatial dependence of the field is proportion to $1/r^2$, i.e. the gradient has a $1/r^3$ dependence on the radial coordinate. Equation (8) indicates that the frequency offset is greater around larger vessels, but that the gradient is greater around smaller ones. The behavior of the spin system in an MR experiment depends crucially on how the diffusion length as defined in eqn (6) is related to the local gradient in the field. If the changes in the field are small over the scale of the diffusion length then signal losses will be predominantly determined by static dephasing. If the changes are large then diffusing spins will experience the full range of external fields, which being symmetrically positive and negative [see eqn (8)] will average zero. This process is often termed dynamic averaging. There will be no net

phase change, and the signal loss will be determined by diffusion effects. Ideally, this problem would be analysed using the Bloch–Torrey equation [see eqn (1)], which in this situation is

$$\frac{\partial \mathbf{M}_{xy}(\mathbf{r},t)}{\partial t} = iK\sin^2\theta\cos(2\phi)\left(\frac{a}{r}\right)^2\mathbf{M}_{xy}(\mathbf{r},t) + D\nabla^2\mathbf{M}_{xy}(\mathbf{r},t) \quad (10)$$

Unfortunately this equation is not amenable to analytical solution. Ogawa *et al.*[23] employed a Monte Carlo simulation to examine this problem, and found that for larger blood vessels static dephasing dominates, whereas for those smaller than about 8 μm radius dynamic averaging largely eliminates dephasing, but the wide range of susceptibility-induced magnetic fields experienced by the spins leads to diffusional signal loss. Other workers have employed similar methods to give a detailed analysis of the contributions of the intra- and extravascular spaces to the fMR signal.[35] A deterministic approach has also been followed to show that the size of activation induced signal changes depends mainly on the blood volume at rest, and on the main magnetic field strength.[36] The dependence on the radius has the important consequence that for smaller vessels the functional sensitivity increases with the square of the main magnetic field strength, but for larger vessels the dependence is only linear.[23] This explains the drive in fMR to use ever increasing main magnetic field strengths—not only is more functional contrast available, but the contribution of the smaller vessels, which will generally be closer to the site of increased neuronal activity, will be increasingly emphasized. This quadratic field-strength dependence will, however, not continue indefinitely as at some (as yet unknown) value of the main field static dephasing will become dominant even for the region about the capillaries.[37] The fast response is believed to originate from the capillary bed[38,39] and should hence show a purely quadratic dependence on the signal intensity.[23] Although very difficult to detect at field strengths of 1.5 T,[40] the FR has been reliably detected at field strengths of 4 T,[39,41] and is reported to be easily detectable in humans at 7 T.[42] The echo-time dependence of the FR has been the subject of some debate, with reports that the amplitude increased[43] or decreased[44] with increasing echo time. An increase is clearly compatible with a T_2* mechanism, but even a decrease can be accounted for in terms of a diffusion related signal loss.[45] The reason for this is that the largest susceptibility-induced field gradient will be induced next to the vessel wall. The static dephasing here will be greatest, but so will the diffusion-induced signal attenuation. The degree of static dephasing has an exponential dependence on the T_2* weighting duration τ, which is *TE* in a gradient-echo experiment, and the asymmetry delay in an asymmetrical spin echo experiment. The dynamic averaging is given essentially by eqn (2), where the time-parameter in the exponent is *TE* for a gradient-echo experiment, and for a spin-echo experiment includes all the relevant delays which constitute $TE + \tau$. Simulations have shown that for the PRESS experiment, as used in Ernst and Hennig[32] and Hennig *et al.*,[44] the amplitude of the FR will decrease with increasing τ, whereas for a gradient-echo experiment, as used in Yacoub *et al.*,[43] the amplitude will increase up to a TE of about 30 ms. Given the inexactitudes of the simulation the FR amplitude in practice could increase up to a *TE* of more than the 45 ms employed in Yacoub *et al.*[43] before decreasing.

In general the experimental evidence supports the thesis that fMR sensitivity increases supra-linearly with increasing field strength, both for the standard fMR experiment[46] and for the fast response.[40] There is hence no reason to doubt that both static and dynamic averaging play a significant role as described in the standard theory. With the move to ever increasing field strengths the contribution of dynamic averaging, i.e. the diffusion-based contrast in fMR, should assume ever greater importance.

Intravoxel incoherent motion (IVIM)

The diffusion-weighted experiment will induce phase-changes in spins moving with a constant velocity. If a spectrum of velocities is present then dephasing will occur, and signal attenuation without a change in phase will be recorded. In terms of measuring diffusion this effect could be regarded as artifactual, but it will be discussed briefly here because of its potential significance in the interpretation of DWI experiments.

The IVIM approach[2,22,47] predicts for low *b*-values of less than 100 s mm^{-2} a non-monoexponential form for the signal intensity plotted against *b*-value. This is considered due to the intravascular contribution. The underlying model considers the vasculature to be represented by connected, straight tubes of random orientation.[22] Depending upon the exact vascular structure the motion-induced signal change within a single stretch of capillary may be coherent or incoherent. In the former situation the direction of flow does not change during the diffusion weighting (this is the intravoxel coherent motion, IVCM case), whereas in the latter the flow is so great, or the diffusion time so long, that a significant change in direction may be expected. Both of these situations may be encountered in practice. Experimentally it has proven somewhat difficult to measure any deviation in standard DWI experiments. This is caused by the low relative volume of the vasculature (not more than 4%), which means that the signal is dominated by extravascular contributions. In measurements which use substances that remain within the intravascular compartment, such as ^{19}F labeled perfluorcarbon blood substitutes,[48] or use intravascular contrast agents in such a

way as to suppress the extravascular signal,[49] it has been possible to convincingly demonstrate non-monoexponential behavior,[48,49] and to show the expected behavior with increasing flow.[49] The simplest IVIM/IVCM model predicted that perfusion could be modeled using a single pseudo diffusion coefficient;[22] unfortunately this did not fit the experimental results, which required more complex interpretation.[50] Furthermore concern was expressed that this method was not capable of measuring true perfusion.[51] Although undoubtedly of significance for the conceptual development regarding the interpretation of diffusion measurements *in vivo*, IVIM/IVCM has not become an established method for perfusion measurement. As most quantitative diffusion measurements acquire the majority of their data at *b*-values greater than 100 s mm^{-2} capillary perfusion does not appear to significantly influence the results of DWI experiments on water.

THE INTERACTION OF THE INTRA- AND EXTRACELLULAR SPACES

As mentioned in the introduction there is a wide range of applications of diffusion imaging including standard DWI, ADC-measurements, trace measurements and diffusion tensor imaging (DTI). It is not the purpose of this text to examine these, and the interested reader is referred to the wide range of reviews[52–61] and books on the subject,[22,26] of which only a fraction could be cited here.

In this section of the review, an attempt is made to address the issues concerning diffusion *in vivo*, excluding any effects caused by the vasculature, as these were examined in the previous section. The challenge that faces almost all fields of biomedical MRI research is to relate the MR-parameter measured to physiological and morphological properties of the object. This is particularly true of diffusion imaging, as brain tissue is capable of dramatic but reversible changes in ADC, depending upon the pathological state. The challenge is to find explanations for the changes in ADC that occur in ischemia and other pathologies, the changes in ADC upon maturation and the mechanism responsible for anisotropy in diffusion. Of these the approximately 40% reduction in ADC recorded within minutes of an ischemic insult has attracted the most attention. In the next section analytical approaches for modeling diffusion *in vivo* will be presented. Then the major experiments that have contributed to a mechanistic understanding will be examined. In the 'Discussion' section the material presented in the previous two sections, which summarize almost a decade of intensive research, will be assessed and discussed.

Analytical and numerical approaches

In the course of time it has become clear that the interaction between the intra- and extracellular compartments is complex, with the respective diffusion coefficients and volume fractions of the compartments, the cell membrane permeability, and compartmental exchange times, the extracellular tortuosity and possibly other mechanisms all playing a part. In this subsection the models will be examined which attempt to model the diffusion behavior for a range of conditions based on known or assumed values for the parameters given above. In the interests of consistency the following notation will be used: as discussed above, the diffusion coefficient varies as a function of diffusion time (τ_D), and so the intra- and extracellular diffusion coefficients will be termed $D_I(\tau_D)$, $D_E(\tau_D)$, respectively, with the values in the absence of restriction (or equivalently in the limit of infinitely short diffusion times) simply referred to as D_I and D_E. The long diffusion time limit for the diffusion coefficient of the whole system, or of one compartment, shall be termed ADC, with a specific diffusion time given as necessary. The intra- and extracellular volume fractions shall be termed α_I and α_E. The membrane permeability is P, and the compartmental exchange times k_I, k_E. The effect of tortuosity, i.e. the effect on the extracellular diffusion of having to circumnavigate the cellular obstructions, is given by[62]

$$D_E(\infty) = \frac{D_E}{\lambda^2} \qquad (11)$$

where λ is the tortuosity.

The aim of all the models presented here is to incorporate differences in the intra- and extracellular diffusion coefficients, the membrane permeability, exchange times and the tortuosity in order to predict the behavior of the system as a whole.

The Latour–Mitra model. This theory has its origins in the treatment of diffusion in porous media. Here spins diffuse through stone by means of interconnected pores; the analogy to the extracellular space *in vivo* is self-evident. The theory as developed for porous media[63,64] still had to be modified for the presence of two diffusing and NMR-detectable compartments separated by a semi-permeable membrane. In the seminal paper to this theory[65] Latour *et al.* present analytical formulae which should predict the ADC both at long and short diffusion times. The system examined is, however, one consisting of packed erythrocytes, and not brain tissue. For short diffusion times the authors present a formula eqn (4) in Latour *et al.*[65] which has previously been derived for porous media.[64] They use a dimensional analysis to show that the formula is applicable to multi-compartment systems separated by permeable membranes provided that the diffusion time is short. Explicitly for a two-

compartment system the short time diffusion coefficients are then given by:

$$D_{\mathrm{I,E}} = D_{\mathrm{I,E}}\left(1 - \frac{4S\sqrt{D_{\mathrm{I,E}}t}}{9V_{\mathrm{I,E}}\sqrt{\pi}}\right) + O(t) \qquad (12)$$

where S/V_{I} and S/V_{E} are the surface to volume ratios for the intra- and extracellular compartments. The signal attenuation for the system as a whole is then obtained by adding the signal decays for the two components, weighted by their respective volume fractions.

Erythrocytes are approximately spherical in form, a problem that is amenable to effective medium theory. This theory is powerful because it implicitly considers the extracellular diffusion pathways, and does not rely on placing the spheres on a periodic lattice. It is used to obtain a formula for the behaviour at long diffusion times[65]

$$\left(\frac{ADC \cdot c_{\mathrm{c}} - D_{\mathrm{I}}c_{\mathrm{I}}}{D_{\mathrm{E}}c_{\mathrm{E}} - D_{\mathrm{I}}c_{\mathrm{I}}}\right)\left(\frac{D_{\mathrm{E}}c_{\mathrm{E}}}{ADC \cdot c_{\mathrm{c}}}\right)^{1/3} = \alpha_{\mathrm{E}} \qquad (13)$$

where

$$D_{\mathrm{I}}c_{\mathrm{I}} = \frac{PaD_{\mathrm{I}}c_{\mathrm{I}}}{Pa + D_{\mathrm{I}}c_{\mathrm{I}}} \qquad (14)$$

and

$$c_{\mathrm{c}} = \alpha_{\mathrm{E}}c_{\mathrm{E}} + \alpha_{\mathrm{I}}c_{\mathrm{I}} \qquad (15)$$

here a is the radius of the spheres, c_{I} and c_{E} are the intra- and extracellular water concentrations. In general it is not considered that concentration differences play a role in determining *in vivo* behavior and they shall not be considered in subsequent models. A similar formula is also given for the diffusion coefficient perpendicular to the long axis of cylindrical cell structures

$$\left(\frac{ADC \cdot c_{\mathrm{c}} - D_{\mathrm{I}}c_{\mathrm{I}}}{D_{\mathrm{E}}c_{\mathrm{E}} - D_{\mathrm{I}}c_{\mathrm{I}}}\right)\left(\frac{D_{\mathrm{E}}c_{\mathrm{E}}}{ADC \cdot c_{\mathrm{c}}}\right)^{1/2} = \alpha_{\mathrm{E}} \qquad (16)$$

This should be of assistance in computing the transverse diffusion coefficient in white matter.

This model utilizes the SGP approximation to derive its results. The authors indicated that the effect of finite gradient pulse length could be corrected for both in the long and the short diffusion time situations.[66] The diffusion behavior at intermediate diffusion times requires a Padé approximation.

The Szafer model. The analytical model developed by Szafer *et al.*[67] is based on diffusion in a regular lattice. These authors took a model consisting of quadratic cells placed in a square matrix. This may at first appear somewhat artificial, but it readily allows the simulation of packing factors similar to those encountered *in vivo*, which for example is not possible if closely packed spheres are examined. Analytical expressions for the ADC in a particular direction are obtained by considering a concentration gradient in this direction, for illustration only diffusion perpendicular to the long axis of the cells will be considered initially. Following earlier workers[68] two approaches are pursued. In the first strips are considered parallel to the gradient direction. The effective diffusion, including the effect of membranes, is calculated for the two types of strip that occur (through the cell or adjacent to it), and the strips are then considered in parallel. This is the series-parallel (*sp*) calculation. In the second approach the strips are initially considered to be perpendicular to the direction of the gradient, i.e. the short pathways through the strip are considered in parallel, and successive strips are then considered to be in series (*ps* approximation). The difference between the two approaches is that in the *ps* approach the pathways do not have to be continuous between the strips. Thus two sets of analytical formulae are obtained in each instance. Quantitatively these yield similar results, and so for the sake of brevity only the *sp* equations will be presented here, as they are slightly more accurate.[67]

$$ADC_{\mathrm{ll}} = \alpha_{\mathrm{I}}D_{\mathrm{I}} + \alpha_{\mathrm{E}}D_{\mathrm{E}} \qquad (17)$$

$$ADC_{\mathrm{pe}} = \left(\frac{\sqrt{\alpha_{\mathrm{I}}}}{\sqrt{\alpha_{\mathrm{I}}}D_{\mathrm{l}} + (1 - \sqrt{\alpha_{\mathrm{I}}})D_{\mathrm{E}}} + \frac{1 - \sqrt{\alpha_{\mathrm{I}}}}{D_{\mathrm{E}}}\right)^{-1} \qquad (18)$$

where in analogy to eqn (14),

$$D_{\mathrm{l}} = \left(\frac{2}{Pl} + \frac{1}{D_{\mathrm{I}}}\right)^{-1} \qquad (19)$$

and the subscripts 'll' and 'pe' denote diffusion parallel and perpendicular to the long axes of the cells, respectively. Here l denotes the cell dimension perpendicular to the long axis. A composite ADC is then given by

$$ADC = \frac{1}{3}ADC_{\mathrm{ll}} + \frac{2}{3}ADC_{\mathrm{pe}} \qquad (20)$$

Results are also presented for a lattice with cubic cells. The authors prefer to employ eqn (20) rather than the cubic lattice, as the former offers the possibility of extended intracellular diffusion pathways. The tortuosity can be calculated theoretically for models of this nature (see Appendix B of Szafer *et al.*[67]), but will in general differ from that found experimentally. The authors correct for this by modifying D_{E} to give the correct contribution of the extracellular diffusion to the ADC. As for the Latour–Mitra model the SGP approximation is also used in these calculations; the authors argue that the results are not significantly affected by using longer gradient pulses provided that δ is smaller than the time scale in which the ADC changes rapidly as function of diffusion time. Analytical formulae are only presented for the long diffusion time scenario, the short diffusion

time regime is examined using a Monte Carlo simulation (see below).

The Stanisz–Szafer model. This is probably the most ambitious model proposed to date.[69] It was specifically developed for diffusion in bovine optic nerve. Both axonal and glial cells are considered with the former being modelled by prolate ellipsoids and the latter by spheres. The intracellular diffusion coefficient is given by[70]

$$D_{\mathrm{I}}(\tau_{\mathrm{D}}) = -\frac{1}{b}\ln\left[2\frac{1-\cos\beta}{\beta^2} + 4\beta^2\sum_{n=1}\frac{1-(-1)^n\cos\beta}{[\beta^2-(n\pi)^2]^2}\exp\left(-n^2\pi^2 D_{\mathrm{I}}\frac{\Delta}{l^2}\right)\right] \quad (21)$$

where

$$\beta = \gamma\delta|\mathbf{G}|l \quad (22)$$

and l is the separation between flat impermeable barriers. This formula is used to calculate values of D_{I} along the main axes of the prolate ellipsoids and in the spheres.

The extracellular diffusion is modeled by the approach of Sen *et al.*,[63] i.e. effective medium theory, also applied in the two models considered above. In contrast to the model of Szafer *et al.*[67] and to the approach of Pfeuffer *et al.*[71] (see below) the tortuosity is calculated directly for diffusion both parallel and perpendicular to the long axes of the prolate ellipsoids. Exchange between the three compartments is calculated according to an extension of the Kärger formalism.[72] A consequence of developing such a complex model is that there are nine free parameters which may be varied.

A similar approach was subsequently followed by Pfeuffer *et al.*[71] They consider only the two standard compartments, without differentiating between different cell types. The cells are considered to be cubic in form. The intracellular diffusion and exchange between compartments are modeled in the same way as by Stanisz *et al.*,[69] but instead of calculating the extracellular tortuosity on a theoretical basis, experimental values are taken from the literature.

In contrast to the Latour–Mitra and Szafer models presented above, the behavior at intermediate diffusion times is explicitly accounted for in this approach. Furthermore the Kärger equations require the exchange rate between the compartments in question and not the permeability. These two parameters are related to each other via the surface-to-volume ratio. However, the exchange time may in principle be determined experimentally for a given system without requiring detailed knowledge of the morphology and membrane permeability, and is hence a parameter that is experimentally more accessible.

Numerical simulations. Given the complexity of the problem, it is not surprising that some workers have utilized numerical simulations to predict the results of diffusion experiments *in vivo*. The first simulation to be considered here is that of Lipinski,[73] which concerns itself exclusively with diffusion in the extracellular space. Images of histological sections were digitized, and used as the basis of Monte Carlo simulations. The size of the cells recorded in the images was permitted to grow or shrink, allowing the volume fraction of the extracellular space to be modified. The result of the simulation gave essentially the extracellular tortuosity as a function of the extracellular volume fraction. In this way it was possible to confirm Archie's law,[63] which had previously been demonstrated experimentally for brain tissue by Nicholson and Philips.[62]

A Monte Carlo simulation pertaining to the diffusion of water in both the intra and extracellular spaces was presented by Szafer *et al.*[67] in the same publication as discussed above. This examined the same model of fibrous tissue as previously discussed and allowed water to diffuse in both spaces, which were permitted to have their own diffusion coefficients and T_2 values. The diffusion between the two compartments was regulated by the membrane permeability and the boundary condition that no net transfer between the compartments may occur. The value of $ADC(\tau_{\mathrm{D}})$ was calculated for diffusion times between 0 and 100 ms for a range of permeabilities and for the two cases that T_2 is equal between compartments and for T_2 significantly longer in the extracellular space. For diffusion perpendicular to the fiber direction there was found to be a strong diffusion time dependence for diffusion times of less than about 20 ms, but for diffusion along the fiber direction there was essentially no diffusion time effect. For impermeable membranes $ADC(\tau_{\mathrm{D}})$ increased as a function of diffusion time when the extracellular space had a longer T_2, simply due to the increased weighting of this space at longer echo times. The authors examine the possible effects of differing T_2 values between the compartments in some detail, and conclude that for realistic permeabilities the effects of T_2 differences are generally negligible. In a subsequent publication the authors found that the Monte Carlo approach is computationally too slow for parameter fitting, and developed the analytical formalism summarised as the Stanisz–Szafer model above.[69]

A model developed to analyse diffusion in white matter is that of Ford *et al.*,[74,75] which was particularly developed to examine injuries to rat spinal chord. This shows certain similarities to that of Szafer *et al.*,[67] but instead of modeling the tissue as consisting of parallel square cells, a circular cross-section is assumed. In the initial version[74] the cylinders are either placed on a square or on an hexagonal matrix and abut each other. In an extension of the original paper, non-abutting cylinders on a hexagonal matrix are also considered, thus allowing for tortuous extracellular pathways.[75] The authors concluded that both changes in cell volume and possible

changes in permeability contribute to measured changes in ADC. They further conclude that, even at the shortest diffusion times reachable in bio-medical MR experiments, significant numbers of water molecules will have impinged on the cell membranes, so that the short time limit for the ADC will only be reachable for diffusion times of under 0.1 μs, which would then correspond to the diffusion times at which eqn (12) is valid.

Experimental studies

This subsection describes some of the experiments that have contributed to the development of the field by determining either the physiological boundary conditions, testing the analytical models described in the previous section, or by offering new insight into the processes that affect the diffusion weighted experiment.

Determination of physiological parameters

Tortuosity. The tortuosity factor λ is a dimensionless quantity that describes how the impermeable barriers within the brain reduce the diffusion coefficient, as compared to the value in the absence of such barriers [cf. eqn (11)]. The rigorous concept of tortuosity as applied to the extracellular space in the brain was first proposed and demonstrated by Nicholson and Phillips[62] by analogy to developments in the theory of porous media.[76] The measurement of tortuosity is generally effected by ionophoresis, i.e. by examining the concentration of ions introduced into the extracellular space as a function of time. The process thus corresponds to Fickian diffusion in the presence of a concentration gradient. The results obtained for rat brain give a value of about 1.6 for adult rats, 1.5 for newborns and 2 post mortem.[77,78]

Intra- and extracellular volume fraction. Of these two parameters the extracellular volume fraction α_E is that most easily measured, α_I being trivially deduced from this. The most commonly used methods for the determination of α_E are ionophoresis (see above) and the measurement of tissue resistance.[79] The tissue resistance method is based on the same Maxwellian model as that used in the analytical models described above, the analogy is the basis for assuming that information regarding the ADC will also yield information concerning the electrical conductivity. Both approaches give values of about 0.2 in the healthy brain. Values of about 0.05 and 0.1 are obtained for cytotoxic edema using the ionopheric method on rats[77] and the resistance method on cats,[80] respectively. The size of the extracellular space in neonates is about double that in the mature brain.[78]

Intra- and extracellular diffusion coefficients. The accurate determination of D_I and D_E is essential for the verification of the models described above. It is, however, by its nature difficult, particularly the determination of the extracellular coefficient: water will exchange between the two compartments and it may not be trivial to derive a value for water based on the diffusion coefficients of substances that remain in one compartments. Some authors have simply taken the values of water or CSF at body temperature to represent the unhindered value of D_E. By using cell cultures it is possible to obtain values for $D_I(\tau_D)$ as first demonstrated by van Zijl *et al.*[81] The cells in such a medium are not so densely packed as *in vivo*, and so at high *b*-values only the signal from the restricted intracellular water will remain. The work of van Zijl *et al.* was improved upon both by using cell types more similar to those in the brain, and by extending the data analysis to allow for the non-zero permeability of the cell membrane. In contrast to the original experiment, a range of cell types have subsequently been examined[82–84] also under conditions of osmotic stress, during which it was possible to document the expected changes in intracellular volume. Within the context of a restricted intracellular environment it is not of primary interest to record the diffusion coefficient of the slowly diffusing compartment for a certain combination of diffusion weighting and diffusion time, as this will at best only yield information concerning the morphology of the cell. That which is of primary interest is the intracellular diffusion coefficient in the absence of restriction, i.e. D_I. The experiments which have come closest to measuring this are those of Pfeuffer *et al.*[84] who applied the formalism as outlined above to analyze their data. The best correspondence with experimental data was obtained for a D_I of about 1.0×10^{-3} mm^2 s^{-1} in some agreement with data obtained from other methods.[85–87]

The difficulties in measuring *in vivo* diffusion characteristics of the two compartments separately using water has led one group of researchers to examine the use of water analogs, which are not expected to readily cross the cell membrane during the diffusion-weighting experiment, and may be confined to one compartment alone. In the first of these experiments ^{133}Cs was employed,[88] this being a potassium analog that accumulates preferentially in the intracellular space. The experiment was performed on rats, and found that the ^{133}Cs ADC decreased from 0.91 to 0.71×10^{-3} mm^2 s^{-1} within 20 min post mortem. In a second experiment on rats 2-[^{19}F]luoro-2-deoxyglucose-6-phosphate (2FDG-6P) was employed.[89] 2FDG was administered intravenously; when taken up by cells in the brain, this substance is metabolized to 2FDG-6P which cannot cross the cell membrane. The same substance can be employed as an extracellular marker via direct intracerebroventricular infusion. The results of these experiments showed that the extracellular ADC fell from 0.144 to 0.086×10^{-3} mm^2 s^{-1} in going from *in vivo* to post mortem. For the intracellular space, similar values of 0.157 and 0.099×10^{-3} mm^2 s^{-1}, respectively, were recorded.

Membrane permeability. Without knowledge of the surface-to-volume ratio it is clearly impossible to determine the permeability. This is in some cases known, for example in the case of erythrocytes. Furthermore, by manipulating the membrane permeability, changes in the diffusion behavior can be induced. Latour *et al.*[65] tested their model on erythrocytes in suspension. Three samples of the same cell type were examined. In one the membrane permeability was reduced by the addition of *p*-chloromercuribenzenesulfonate which inhibits transport through the pores in the membrane. In another sample the cell volume was increased by reducing the saline concentration of the extracellular medium. The measured permeability corresponded well to expectation for the control sample, and for that with reduced permeability, but was significantly overestimated for the sample with increased intracellular volume. Pfeuffer *et al.*[90] examined a variety of cell types under conditions of osmotic stress also in the presence of mercury chloride as a blocker of water channels, and came to the conclusion that water transport in glial cells is mainly via these channels.

Exchange times. As has previously been mentioned, the surface-to-volume ratio for the cell types found in the brain is not easily determined. Analytical models which utilize the Kärger formulation, however, require only the exchange time, and so there is considerable interest in measuring these. Following the method of Andrasko,[91] who measured the exchange time of humane erythrocytes to be 17 ms at 297 K, Pfeuffer *et al.* performed a number of measurements on cell suspensions and recorded values of about 50 ms at 310 K for F98 glioma cells, primary astrocytes and epithelial KB cells.[84] This method was subsequently extended to imaging experiments on the rat brain giving an upper value of 15.4 ms.[71] Subsequent work from the same group has argued that the measured exchange time increases with diffusion time[92] and has given an *in vivo* exchange time of 578 ms for a diffusion time of $\geq$780 ms. This latter value corresponds closely to that previously recorded by Duong *et al.*[93] using a completely different approach. Here a gadolinium based contrast agent was introduced into the extracellular space of the rat brain, so that a significant T_1 difference existed between the two compartments. The data were then fitted to a two-compartment exchange model yielding values of 610 ± 100 and 230 ± 90 ms for the intracellular and extracellular exchange times respectively.

Experiments at high *b*-value or short diffusion time. Experiments which measure the ADC *in vivo* almost always yield mono-exponential decay curves. This can be seen as an advantage, as it implies that over a wide range of experimental conditions the diffusion characteristics in tissue can be described by a single decay constant. However, under conditions of high *b*-value or short diffusion time it is possible to demonstrate marked deviations from mono-exponentiality, and these experiments will be described here.

Initial tests of the diffusion-time dependence of the ADC had suggested that it was invariant on the diffusion time,[94,95] at least for values between 17 and 2000 ms. Further experiments, however, demonstrated a significant decrease in ADC for human brain tissue[96] using diffusion times of between 40 and 800 ms, and *b*-values up to about 2200 s mm^{-2}. These data are indicative of restricted diffusion.

Subsequent to this experiment rat brain was investigated *in vivo* using a significantly greater range of *b*-values.[97] The data could be well fitted to a biexponential curve, however the relative sizes of the fast- and slow-diffusing components was the opposite to that expected from the relative volumes of the intra- and extra-cellular compartments. The curves showed no diffusion time dependence for diffusion times between 8 and 60 ms. The authors also showed that their data could not be modeled using the standard Kärger exchange model.[72] Similar experiments have recently been performed on the human brain, and have given similar results.[98] Experiments on excised brain tissue with a still greater range of *b*-values[99] (up to 3×10^4 s mm^{-2}) did then, however, demonstrate a clear diffusion time dependence over the same range of diffusion times as in Niendorf *et al.*[97] At this range of *b*-values the data could only be modeled successfully using a three component exponential fit.[99] In the most recent data, here obtained under *in vivo* conditions from a rat brain[100] with *b*-values up to 7×10^4 s mm^{-2} a continuous distribution of diffusion coefficients is allowed, which however are resolvable into three main peaks. It should be noted that these three peaks are not the same as the three components of the tri-exponential fit described in Assaf *et al.*[99]

The model developed by Stanisz *et al.*[69] and described above was primarily developed to account for the data obtained from excised bovine optic nerve. Their model is complex, having nine free parameters, and was applied for a range of *b*-values up to 4×10^4 s mm^{-2}, i.e. comparable to the range used in the other experiments described above. It is of interest to note that the analytical form of the curve used here does not rely on a sum of exponential decays, and gives a good fit to their own data.

The effects of restriction may be detected not only at high *b*-value but also at short diffusion times. Technical limitations generally mean that such experiments are performed with a limited range of *b*-values. Restriction manifests itself as a difference in signal attenuation for the same *b*-value at differing diffusion times. In its simplest form the Stejskal–Tanner experiment is implemented so that the gradient strength is held constant and the *b*-value varied by modifying δ, and thus simultaneously modifying the diffusion time while keeping the echo time constant. Comparison of this *cg* experiment with a standard *ct* experiment in which all timings are held constant and the *b*-value is varied by the gradient

strength gives evidence of restriction for diffusion times up to about 10 ms.[101–103] In an extension of this experiment the *b*-value is held constant and the diffusion time varied (*cb* experiment). Using these experiments it was found that at diffusion times of between 1.8 and 6 ms both healthy and post mortem brain tissue shows evidence of restriction. For cytotoxic edema restriction is also visible at longer diffusion times (4.5–11.8 ms). The ADC as determined by the standard *ct* experiment was found to vary between 1.1×10^{-3} mm^2 s^{-1} at a diffusion time of 6 ms and 0.89×10^{-3} mm^2 s^{-1} at 11.8 ms. It was found to be possible to interpret these results in accordance with changes in the extracellular tortuosity.[103]

Examinations of pathological models. Numerous experiments have been performed to examine changes in diffusion characteristics under controlled pathological conditions. Following the initial reports of a dramatic decrease in ADC following cerebral ischemia[5] considerable effort was invested in developing methods whereby occlusion could take place within the magnet.[104] It was thus possible to follow the time course in detail starting at the time of ischemia both for focal and global ischemia. It was found that the ADC can start to fall dramatically within 2 min of global ischemia being induced via cardiac arrest,[105] and that the decline is biphasic, with an initial rapid fall of about 40% within minutes, followed by a continuous gradual decline attributed to a drop in temperature.[106] Over longer time periods it was found that the ADC returns to control value at between 48 and 72 h.[107,108]

An important pathology that also shows changes in ADC is epilepsy. In a study of bicuculline-induced *status epilepticus* in rats a drop in ADC was found of about half that encountered in severe ischemia.[109] In contrast to cerebral ischemia blood flow is greatly increased and ATP only moderately depleted: cell swelling is, however, common to both states.

It is of course possible to add substances to the extracellular space that induce a cell swelling. In the first experiment of this nature[110] exposure to ouabain, glutamate and *N*-methyl-D-aspartate (NMDA) was compared to middle cerebral artery occlusion (MCAO). Ouabain inhibits Na, K-ATPase so that these pumps fail, causing the cells to swell. Glutamate and NMDA are both excitotoxins which also cause cell swelling. In all cases a 30–40% reduction in ADC was observed.

Cortical spreading depression may be induced by the direct application of KCl to the brain, and results in a wave of cell depolarization that spreads along the cortex of the rat brain at a speed of about 3 mm/min.[111] It has been shown to be possible to visualize this wave using DWI,[112–114] as the depolarization results in a reversible cell swelling similar to that encountered in ischemia.

In order to understand the causal relationships that lead to a fall in ADC it is important to characterize the time-course of events that occur immediately after the onset of ischemia. By means of ionophoric measurement of the extracellular space it was possible to show that in rats the major reduction in extracellular volume occurs simultaneously with the onset of anoxic depolarization.[111] An imaging study of both focal and global ischemia in the rat show that ADC changes are decoupled from the changes in DC-potential by examining differences in the time course of the latter parameter between the two types of ischemia: the changes in ADC were observed to be not significantly dependent on the type of ischemia used.[115] The ADC changes occurred prior to the depolarization. This data corroborates previous experiments which also found an earlier than expected reduction in ADC.[116,117] These results are, however, not unequivocal as they are contradicted by a short study that combined DWI with electrophysiological measurement and found a coincidence between the onset of depolarization and changes in MR signal intensity.[118] Furthermore it could be shown by combining ionophoric methods and MR investigations that the time course of ADC changes closely follows that of changes in cell volume and extracellular tortuosity over the period up to 2 min following global ischemia.[119]

One result common to all these experimental models is that ADC changes are reversible, provided that widespread cell death does not occur.

Examinations of anisotropy and maturation. Cell processes which have a preferred orientation, and are ordered on the scale of an imaging voxel exhibit anisotropic diffusion. This applies to white matter in the brain, and its effect on DWI images was demonstrated at an early stage.[120,95] Since the initial publications demonstrating diffusion tensor imaging DTI,[16–18] this area has developed rapidly, and shows enormous potential for fiber-tracking *in vivo*.[121,122] The mechanism responsible for the anisotropy has been investigated in a number of publications. It was found that the non-myelinated olfactory, and the myelinated trigeminal and optic nerves of garfish all exhibited similar degrees of anisotropy,[123] in a further experiment using the giant axon of the squid it was shown that neurofilaments do not contribute to diffusion anisotropy, and hence that restriction caused by the membrane must be decisive.[124] In the most recent experiments performed on both myelinated and non-myelinated nerves,[125] signal from the various compartments was separated on the basis of T_2, with the shortest T_2 being assigned to water in the myelin (where present), the next shortest T_2 to intracellular water and the longest T_2 to extracellular water. All three of these compartments show anisotropic behavior. These results confirm those of earlier studies which showed that in rat pups the presence of anisotropy predated that of myelination,[126] and that in mutant mouse strains where myelination of the optic and trigeminal nerves is impaired the anisotropy is still the same as in healthy mice.[127]

Studies performed on newborn humans[128,129] and

cats[130] show a consistent picture of elevated ADC in newborns compared to the adult. The reduction in ADC shows a significant correlation with increasing gestational age,[129] and the concomitant reduction in T_2.[130] In one study the anisotropy was found to increase with increasing gestational age,[128] whereas in the other study a significant correlation was only found for the centrum semiovale.[129] These results are generally consistent with increasing cell density and myelination resulting in a reduction in the size of the extracellular space. Indeed, experiments have been performed on neonatal rats to exploit this enlarged extracellular space and the associated reduction in tortuosity.[97] The results have generally conformed to expectation in that as the extracellular space has shrunk and the tortuosity increased the ADC has fallen.

Discussion

The discussion is so structured that the development of the consensus theory is first described. Explanations for various experimental results in the light of this will then be given. The difficulties associated with attempting to produce quantitative results from models which incorporate the essential features of the theory will then be examined. Finally, the interpretation of recent experimental work that would appear to contradict the consensus theory is discussed.

In the original paper describing the efficacy of DWI in detecting cerebral ischemia[5] possible causes of the change in ADC were given as temperature changes, motion and cell volume changes, with the latter seeming the most credible. A further suggestion concerned a reduction in convective streaming within the cell.[131] The involvement of cell swelling received rapid experimental support in the form of the experiments performed by Benveniste *et al.*[110] as described above. The alternative suggestion that changes in membrane permeability could be responsible,[132] while being at first sight physically credible was generally considered implausible on physiological grounds. Furthermore the theoretical work described above clearly showed that for physiological values the results would be largely insensitive to further reductions in permeability. Early theories based on there being no evidence of restriction at long diffusion times, but clear evidence for this at short diffusion times,[103] were superseded with the discovery of clear evidence for restriction at high *b*-values.[96] Qualitative[103] and quantitative theories[65,67] emerged implicating extracellular tortuosity as being an important additional factor contributing to the change in ADC. There thus emerged a general consensus that the changes in ADC detected in cerebral ischemia were caused by a combination of a water shift from the extra- to the intracellular space, coupled with an increase in extracellular tortuosity. This hypothesis was qualitatively supported by a large number of experimental studies, including many of those mentioned above. The physical situation was most aptly described in Stanisz *et al.*[69] as 'tissue can be regarded as roughly independent intracellular and extracellular compartments which are weakly coupled through the cellular membranes'.

This consensus theory can qualitatively explain the experimental results given earlier. In *status epilepticus* the reduction in ADC is accompanied by cell swelling, and the higher ADC found in the post-natal brain correlates well with the larger extracellular volume and lower extracellular tortuosity in this tissue. Based on the work described above there is also a clear explanation for the origins of anisotropy: as predicted[103] the diffusion in both the intra- and extracellular spaces will be anisotropic. The increased impermeability of the cell membrane due to myelination is not of great significance here, as shown in the simulation of Szafer *et al.*[67] where decreases in the permeability beyond that expected for an unmyelinated cell have little effect on the diffusion characteristics. The main effect of demyelination would then be to reduce the tortuosity of the extracellular space.

It would however be misleading to represent this consensus theory as being complete, as it should then lead to quantitatively accurate predictions of the diffusion behavior over the complete range of diffusion times and *b*-values. This may be possible, but a full range of tests has to date not been performed, and certain limitations in the mathematical models must be considered.

If we examine first the Latour–Mitra model described earlier then it has to be borne in mind that in the limit of long diffusion times this model deals explicitly with either a spherical or a cylindrical cell geometry: as stated by the authors themselves this will only yield qualitatively correct results for other geometries. This can be emphasized by examining Appendix B of Szafer *et al.*[67] from which the extracellular tortuosity for an extracellular volume fraction of 0.2 in a suspension of spheres may be calculated as 1.06, and perpendicular to the long axis of a random array of cylinders as 1.18. Both these values are significantly different from the measured values of about 1.6 obtained for tissue in practice.[77,78] This caveat is supported by results presented within the article itself: the authors calculate a percentage change in ADC in going from healthy to infarcted tissue that corresponds closely with the experimental results; however the absolute ADC values calculated differ significantly from experiment.[65] The short diffusion time formula presented in this paper [eqn (4)] is of more general applicability, but again as pointed out by the authors, and supported by the simulation results of Ford *et al.*,[74,75] this almost certainly represents a regime that is currently experimentally inaccessible.

The work of Szafer *et al.* as discussed above covers both analytical expressions for the long diffusion time limit, and Monte Carlo simulations which cover a range

of diffusion times, and converge in the short time limit to that presented by Latour *et al.*[69] With these it is possible to account for the changes in ADC measured at short diffusion times as described earlier. It is also shown that if the membrane permeability were close to zero then the intracellular diffusion coefficient would have to have a value which is unrealistically low. The authors discuss the possibility that the extracellular tortuosity of water may be lower than that of the macromolecules used to experimentally determine this parameter. In this situation they are capable of calculating ADC values for both healthy and infarcted tissue that correspond well with experiment. If they follow the more conventional assumption that for small molecules tortuosity values are independent of molecular size, then they have to assume a larger than expected intracellular diffusion coefficient of $1.5 \times 10^{-3}\,\mathrm{mm^2\,s^{-1}}$, and significantly, in the light of the discussion below, a reduction in D_I for cytotoxic edema.

In the Stanizz–Szafer model presented above the parameter fit yields a value for the average intracellular diffusion coefficient of $1.12 \times 10^{-3}\,\mathrm{mm^2\,s^{-1}}$ with the extracellular tortuosity being calculated analytically. As the extracellular space is different in bovine optic nerve than in brain tissue the results may not readily be compared. An important point to note is that the authors are only able to fit their experimental results if they include both types of cell, considering only the axons is completely inadequate for modeling their data. This leads to the necessity of having two different exchange times for the axonal and glial cells. Even in models of cell cultures it has been found necessary to include a Gaussian distribution of cell sizes.[133] The situation in brain tissue, where large voxels effectively average over multiple white-matter orientations, will be even more complex, and could explain why attempts to measure exchange times using diffusion methods have led to inconclusive results.[71,92]

In assessing the analytical models, it would seem that the approach most likely to succeed is to model the intracellular spaces as described by Stanisz *et al.*,[69] as this allows both for spheres and prolate ellipsoids, the extracellular tortuosity may then either be calculated, or more pragmatically experimentally determined values taken, as done by Szafer *et al.*[67] and by Pfeuffer *et al.*[133] It is likely that a model of this nature would fit much of the experimental data, for example that acquired by Niendorf *et al.*[97] and Assaf and Cohen.[99] This would avoid multi-exponential fitting where the individual exponential components obtained bear no direct relation to any physiological compartments.

The analytical approach is capable of giving a good fit to experimental data, provided that the model is sufficiently complex. There are then a large number of free parameters, and if these are not independently known then the stability of the fit may be problematic. Furthermore, a good fit in itself does not necessarily imply that the model is physically or physiologically correct, as there may be no independent means of verifying if the parameter values that give this fit are themselves correct and not just plausible. The idea of accounting for all diffusion characteristics on the basis of changes in cell volume and extracellular tortuosity is called into question by the problems encountered by Szafer *et al.*[67] in predicting the ADCs of normal and infarcted tissue, and of Stanisz *et al.*[69] in obtaining a good and stable fit to all their experimental data. It is not clear whether the requirement of Szafer *et al.*[67] for a significant reduction in D_I is genuine or arises from the simpler nature of his model compared to that of Stanisz *et al.*[69]

Further problems with the consensus model arise when the results of the experiments which use ^{133}Cs and 2FDG-6P to evaluate intracellular,[88,89] and 2FDG-6P to evaluate extracellular[89] diffusion coefficients are considered. The first problem to contend with is that intra- and extracellular diffusion coefficients are similar, the second is that post mortem they fall by a similar amount. The evidence for a drop in intracellular diffusion coefficient is supported by results from diffusion spectroscopy.[134–136] The diffusion coefficient of ^{133}Cs in aqueous solution is similar to that of water itself. The value measured *in vivo* is $0.9 \times 10^{-3}\,\mathrm{mm^2\,s^{-1}}$ at a diffusion time of 27 ms measured for a *b*-value range of up to $1400\,\mathrm{s\,mm^{-2}}$ i.e. about a third of its value in aqueous solution at the same temperature. It should be noted that the short gradient pulse approximation did not apply in this experiment ($\Delta = 36$ ms, $\delta = 28$ ms), and hence the theories presented above would have to be modified to fit this data. However for low *b*-values it is to be expected that the signal decay should still be exponential, which is in agreement with the experimental results, and a change in the ADC can then only be caused by a change in the intracellular diffusion coefficient. A fall in ADC of 30% is measured in the transition from *in vivo* to post mortem conditions, exactly as required by the model of Szafer *et al.*[67] for the situation in which the extracellular tortuosity of water is identical to that of small macromolecules.

The interpretation of the 2FDG-6P experiments is more contentious. One open question is the degree to which 2FDG-6P is bound to large macromolecules *in vivo*. It has been argued that as the ratio of ADC values between saline solution and brain is similar for 2FDG-6P and water, that 2FDG-6P must be in the aqueous compartment.[89] However, the ADC of water reflects interaction between the two compartments via the cell membrane, which is absent for 2FDG-6P. It is hence more relevant to compare the ADC changes for the two compartments separately. The intracellular diffusion coefficient at a diffusion time of 24.5 ms and *b*-values of up to $6000\,\mathrm{s\,mm^{-2}}$ was measured as $0.157 \pm 0.021 \times 10^{-3}\,\mathrm{mm^2\,s^{-1}}$ as compared with $0.7 \times 10^{-3}\,\mathrm{mm^2\,s^{-1}}$ in saline solution at 37°C. This represents a drop of 80% in going from saline solution to *in vivo* conditions, far greater than for ^{133}Cs. The relative drop in

ADC value in going from *in vivo* to post mortem conditions is 37%, i.e. similar to that obtained for ^{133}Cs.

The extracellular ADC measured at a diffusion time of 22.2 ms and over the same range of *b*-values is $0.144 \pm 0.018 \times 10^{-3}$ mm^2 s^{-1}. This implies an extracellular tortuosity of 2.2 significantly greater than for water. If, alternatively, it were assumed that the diffusion is free then the diffusion length for this diffusion time would be about 4 μm, easily larger than the dimension of the extracellular space, and hence unlikely. Post mortem the ADC falls to $0.086 \pm 0.012 \times 10^{-3}$ mm^2 s^{-1}, which corresponds to an increase in tortuosity from 2.2 to 2.85, i.e. of a factor 1.3. For small macromolecules (and presumably water) the increase is from 1.6 to 2.2, which gives a similar factor for the relative increase of 1.38.[77]

The interpretation of the combined results for ^{133}Cs and 2FDG-6P is not entirely straightforward. The most likely explanation, as convincingly argued by the authors, for the reduction in intracellular ADC measured in both experiments, is a reduction in intracellular streaming (see Duong *et al.*,[89] and references contained therein). Their results are not compatible with the ADC change being linked with a change in membrane permeability, as the membrane is largely impermeable to these substances prior to any ischemic insult. As the gyromagnetic ratio for ^{19}F is significantly larger than for ^{133}Cs a far higher range of *b*-values is available for the experiments with ^{19}F. The data could, however, only be measured at four *b*-values, and so despite giving a good fit to a monoexponential decay it is unclear to what extent restriction has reduced the ADC. An alternative explanation for the low intracellular ADC value could be that the 2FDG-6P is not in the aqueous compartment. This interpretation is consistent both with the higher than expected extracellular tortuosity and the much larger percentage fall in the intracellular diffusion coefficient in going from aqueous solution to *in vivo* conditions than recorded for ^{133}Cs. The similarity between the pre- and post mortem intra- and extracellular 2FDG-6P diffusion coefficients would then be purely fortuitous.

An interpretation of the data on the lines given above does not resolve all difficulties for the model of Szafer *et al.*[67] This is because the value of the intracellular diffusion coefficient for water if assumed to be identical to that for ^{133}Cs (0.9×10^{-3} mm^2 s^{-1}) or that fitted by Stanisz *et al.*[69] (1.12×10^{-3} mm^2 s^{-1}) will not give a correct value for the ADC of healthy brain tissue as modeled by Szafer *et al.*[67] Both these values are considerably lower than the 1.5×10^{-3} mm^2 s^{-1} which is then required. It is however notable that Stanisz *et al.*[69] are capable of modeling healthy tissue without having such a high value for the intracellular diffusion coefficient. Application of this model to brain tissue and ischemia would hence be of great importance.

A further challenge to the consensus model would be posed if it could be unequivocally shown that changes in ADC are measured in ischemia before changes in cell volume. There is considerable experimental evidence that ADC changes occur before cell depolarisation has taken place.[115–117] However, the only published data which directly measured extracellular volume and ADC during this initial period post-ischemia showed a good correlation between the time course of the volume changes and the ADC reduction.[119] One as yet unresolved issue is, given that there may be a significant reduction in D_I, it is not known what the time scale for this change may be. It could be possible that this reduction occurs before depolarization has taken place.

In summary, there is now convincing evidence for the argument that the following factors play a role in determining ADC:[137] the relative volume of the two compartments, the extracellular tortuosity, intracellular micro-streaming. It is now necessary to re-examine the models initially developed to account for the first two of these factors to see if they are capable of computing ADC values that agree with experiment when a 30% drop in D_I post mortem is incorporated, and to examine the nature and time course of the drop in D_I.

CONCLUSION

The effects of microscopic tissue parameters such as susceptibility gradients, capillary flow, the presence of semi-permeable membranes and the extracellular tortuosity on MR imaging experiments have been described in detail. It has been shown that these microscopic parameters can affect both MR experiments that have been purposely sensitized to diffusion, and those that have a long echo time such as are used in fMR. The theoretical models available can model the experimental data moderately well for all of these situations. The limitations of the models are those general to modeling complex systems using a small number of parameters. To date, the vast majority of experiments have been performed on tissue of the CNS, but as problems associated with motion are surmounted, the extension to other organs becomes more feasible.

Acknowledgements

The author would like to thank Mike Moseley (Stanford), Chris Boesch (Berne), D. Y. von Cramon and Sandra Vos (Leipzig) for helpful comments regarding this text.

REFERENCES

1. Taylor DG, Bushell MC. The spatial mapping of translational diffusion coefficients by the NMR imaging technique. *Phys. Med. Biol.* 1985; **30**: 345–349.
2. Le Bihan D, Breton E, Lallemand D, Grenier P, Cabanis E, Laval-Jentet M. MR Imaging of intravoxel incoherent motions:

application to diffusion and perfusion in neurologic disorders. *Radiology* 1986; **161**: 401–407.
3. Hahn EL. Spin echoes. *Phys. Rev.* 1950; **80**: 580–594.
4. Carr HY, Purcell EM. Effects of diffusion on free precession in nuclear magnetic resonance experiments. *Phys. Rev.* 1954; **94**: 630–638.
5. Moseley ME, Cohen Y, Mintorovitch J, Chileuitt L, Shimizu H, Kucharczyk J, Wendland MF, Weinstein PR. Early detection of regional cerebral ischemia in cats: comparison of diffusion- and T_2-weighted MRI and spectroscopy. *Magn. Reson. Med.* 1990; **14**: 330–346.
6. Mintorovitch J, Moseley ME, Chileuitt L, Shimizu H, Cohen Y, Weinstein PR. Comparison of diffusion- and T_2-weighted MRI for the early detection of cerebral ischemia and reperfusion in rats. *Magn. Reson. Med.* 1991; **18**: 39–50.
7. Moseley ME, Kucharczyk J, Mintorovitch J, Cohen Y, Kurhanewicz J, Derugin N, Asgari H, Norman D. Diffusion weighted MR imaging of acute stroke: correlation with T_2-weighted and magnetic susceptibility-enhanced MR imaging in cats. *Am. J. Neuroradiol.* 1990; **11**: 423–429.
8. Warach S, Chien D, Li W, Ronthal M, Edelman RR. Fast magnetic resonance diffusion-weighted imaging of acute human stroke. *Neurology* 1992; **42**: 1717–1723.
9. Ordidge RJ, Helpern JA, Qing ZX, Knight RA, Nagesh V. Correction of motional artifacts in diffusion-weighted MR images using navigator echoes. *Magn. Reson. Imag.* 1994; **12**: 455–460.
10. Anderson AW, Gore JC. Analysis and correction of motion artifacts in diffusion weighted imaging. *Magn. Reson. Med.* 1994; **32**: 379–387.
11. Butts K, de Crespigney A, Pauly JM, Moseley M. Diffusion-weighting interleaved echo-planar imaging with a pair of orthogonal navigator echoes. *Magn. Reson. Med.* 1996; **35**: 763–770.
12. Wider G, Dötsch V, Wüthrich K. Self-compensating pulsed magnetic-field gradients for short recovery times. *J. Magn. Reson. A* 1994; **108**: 255–258.
13. Jezzard P, Barnett AS, Pierpaoli C. Characterization of and correction for eddy current artifacts in echo planar diffusion imaging. *Magn. Reson. Med.* 1998; **39**: 801–12.
14. Horsfield MA. Mapping eddy current induced fields for the correction of diffusion-weighted echo planar images. *Magn. Reson. Imag.* 1999; **17**: 1335–1345.
15. Koch M, Norris DG. An assessment of eddy current sensitivity and correction in single-shot diffusion weighted imaging. *Phys. Med. Biol.* 2000; **45**: 3821–3832.
16. Basser PJ, Mattiello J, Le Bihan D. MR Diffusion tensor spectroscopy and imaging. *Biophys. J.* 1994; **66**: 259–267.
17. Basser PJ, Mattiello J, Le Bihan D. Estimation of the effective self-diffusion tensor from the NMR spin-echo. *J. Magn. Reson.* 1994; **103B**: 247–254.
18. Mattiello J, Basser PJ, Le Bihan D. Analytical expressions for the *b*-matrix in NMR diffusion imaging and spectroscopy. *J. Magn. Reson.* 1994; **108A**: 131–141.
19. Basser PJ, Pierpaoli C. A simplified method to measure the diffusion tensor from seven MR images. *Magn. Reson. Med.* 1998; **39**: 928–34.
20. Pierpaoli C, Jezzard P, Basser PJ, Barnett A, Di Chiro G. Diffusion tensor MR imaging of the human brain. *Radiology* 1996; **201**: 637–48.
21. Garrido L, Wedeen VJ, Kwong KK, Spencer UM, Kantor HL. Anisotropy of water diffusion in the myocardium of the rat. *Circulation Res.* 1994; **74**: 789–93.
22. Le Bihan D, Breton E, Lallemand D, Abin M-L, Vignaud J, Laval-Jeantet M. Separation of diffusion and perfusion in intravoxel incoherent motion MR imaging. *Radiology* 1988; **168**: 497–505.
23. Ogawa S, Menon RS, Tank DW, Kim S-G, Merkle H, Ellermann JM, Ugurbil K. Functional brain mapping by blood oxygenation level-dependent contrast magnetic resonance imaging. A comparison of signal characteristics with a biophysical model. *Biophys. J.* 1993; **64**: 803–812.
24. Bradbury MWB, Patlak CS, Oldendorf WH. Analysis of brain uptake and loss of radiotracers after intracarotid injection. *Am. J. Physiol.* 1975; **229**: 1110–1115.
25. Patlak CS, Fenstermacher JD. Measurements of dog blood–brain transfer constants by ventriculocisternal perfusion. *Am. J. Physiol.* 1975; **239**: 877–884.
26. Callaghan PT. Principles of Nuclear Magnetic Resonance Microscopy. Oxford University Press: Oxford, 1991.
27. Price WS. Pulsed-field gradient nuclear magnetic resonance as a tool for studying translational diffusion. 1. Basic theory. *Concepts Magn. Reson.* 1997; **9**: 299–336.
28. Torrey HC. Bloch equations with diffusion terms. *Phys. Rev.* 1956; **104**(3): 563–565.
29. Stejskal EO, Tanner JE. Spin diffusion measurements: spin echoes in the presence of a time-dependent field gradient. *J. Chem. Phys.* 1965; **42**: 288–292.
30. Ogawa S, Tank DW, Menon R, Ellerman J, Kim S-G, Merkle H, Ugurbil K. Intrinsic signal changes accompanying sensory stimulation: Functional brain mapping with magnetic resonance imaging. *Proc. Natl Acad. USA* 1992; **89**: 5951–5955.
31. Kwong KK, Belliveau JW, Chesler DA, Goldberg IE, Weisskoff RM, Poncelet BP, Kennedy DN, Hoppel BE, Cohen MS, Turner R et al. Dynamic magnetic resonance imaging of human brain activity during primary sensory stimulation. *Proc. Natl Acad. Sci. USA* 1992; **89**: 5675–5679.
32. Ernst T, Hennig J. Observation of a fast response in functional MR. *Magn. Reson. Med.* 1994; **32**: 136–149.
33. Ogawa S, Lee TM, Kay AR, Tank DW. Brain magnetic resonance imaging with contrast dependent on blood oxygenation. *Proc. Natl Acad. Sci. USA* 1990; **87**: 9868–9872.
34. Ogawa S, Lee T, Nayak AS, Glynn P. Oxygenation-sensitive contrast in magnetic resonance image of rodent brain at high magnetic fields. *Magn. Reson. Med.* 1990; **14**: 68–78.
35. Boxerman JL, Bandettini PA, Kwong KK, Baker JR, Davis TL, Rosen BR, Weisskoff RM. The intravascular contribution to fMRI signal change: Monte Carlo modeling and diffusion-weighted studies in vivo. *Magn. Reson. Med.* 1995; **34**: 4–10.
36. Bandettini PA, Wong EC. Effects of biophysical and physiologic parameters on brain activation-induced R_2* and R_2 changes: simulations using a deterministic diffusion model. *Int. J. Imag. System Technol.* 1995; **6**: 133–152.
37. Ugurbil K, Ogawa S, Kim S-G, Hu X, Chen W, Zhu X-H. Imaging brain activity using nuclear spins. In Magnetic Resonance and Brain Function: Approaches from Physics; Maraviglia B (eds); Elsevier: Amsterdam, 1999.
38. Malonek D, Grinvald A. Interactions between electrical activity and cortical microcirculation revealed by imaging spectroscopy: implications for functional brain mapping. *Science* 1996; **272**: 551–554.
39. Menon RS, Ogawa S, Hu X, Strupp JP, Anderson P, Ugurbil K. BOLD based functional MRI at 4 T includes a capillary bed contribution: echo-planar imaging correlates with previous optical imaging using intrinsic signals. *Magn. Reson. Med.* 1995; **33**: 453–459.
40. Yacoub E, Hu X. Detection of the early negative response in fMRI at 1.5 Tesla. *Magn. Reson. Med.* 1999; **41**: 1088–1092.
41. Hu X, Le TH, Ugurbil K. Evaluation of the early response in fMRI in individual subjects using short stimulus duration. *Magn. Reson. Med.* 1997; **37**: 877–884.
42. Yacoub E, Vaughan T, Adriany G, Andersen P, Merkle H, Ugurbil K, Hu X. Observation of the initial "dip" in fMR signal in human visual cortex at 7 Tesla. *Proceedings: 9th Meeting of the International Society of Magnetic Resonance in Medicine, Denver*, 2000; 991.
43. Yacoub E, Le TH, Ugurbil K, Hu X. Further evaluation of the initial negative response in functional magnetic resonance imaging. *Magn. Reson. Med.* 1999; **41**: 436–441.
44. Hennig J, Janz C, Speck O, Ernst T. Functional spectroscopy of brain activation following a single light pulse: examination of the mechanisms of the fast initial response. *Int. J. Imaging System Technol.* 1995; **6**: 203–208.
45. Dymond RC, Norris DG. Mechanism and echo time dependence of the fast response in fMR. *Magn. Reson. Med.* 1997; **38**: 1–6.
46. Barker PB, Blackband SJ, Chatham JC, Soher BJ, Samphilipo MA, Magee CA, Hilton JD, Strandberg JD, Anderson JH. Quantitative proton spectroscopy and histology of a canine brain tumor model. *Magn. Reson. Med.* 1993; **30**: 458–464.
47. Le Bihan D. Intravoxel incoherent motion imaging. In *Diffusion*

and Perfusion Magentic Resonance Imaging; Le Bihan D (ed); Raven Press: New York, 1995.
48. Neil JJ, Ackerman JJH. Detection of pseudodiffusion in rat brain following blood substitution with perfluorcarbon. *J. Magn. Reson.* 1992; **97**: 194–201.
49. Neil JJ, Bosch CS, Ackerman JJ. An evaluation of the sensitivity of the intravoxel incoherent motion (IVIM) method of blood flow measurement to changes in cerebral blood flow. *Magn. Reson. Med.* 1994; **32**: 60–65.
50. Henkelman RM, Neil JJ, Xiang QS. A quantitative interpretation of IVIM measurements of vascular perfusion in the rat brain. *Magn. Reson. Med.* 1994; **32**: 464–469.
51. Henkelman RM. Does IVIM measure classical perfusion? *Magn. Reson. Med.* 1990; **16**: 470–475.
52. Beaulieu C, D'Arceuil H, Hedehus M, de Crespigny A, Kastrup A, Moseley ME. Diffusion-weighted magnetic resonance imaging: theory and potential applications to child neurology. *Sem. Pediatr. Neurol.* 1999; **6**: 87–100.
53. Horsfield MA, Larsson HB, Jones DK, Gass A. Diffusion magnetic resonance imaging in multiple sclerosis. *J. Neurol. Neurosurg. Psychiat.* 1998; **64**(Suppl 1): S80–84.
54. Mori S, Barker P. Diffusion magnetic resonance imaging: its principles and applications. *Anat. Rec. (New Anat.)* 1999; **257**: 102–109.
55. Rowley HA, Grant PE, Roberts TP. Diffusion MR imaging. Theory and applications. *Neuroimag. Clin. N. Am.* 1999; **9**: 343–61.
56. Norris DG, Niendorf T. Interpretation of DW-NMR data: dependence on experimental conditions. *NMR Biomed.* 1995; **8**: 280–288.
57. Hoehn-Berlage M. Diffusion-weighted NMR imaging: application to experimental focal cerebral ischemia. *NMR Biomed.* 1995; **8**: 345–358.
58. Moseley ME, Butts K, Yenari MA, de Crespigny A. Clinical aspects of DWI. *NMR Biomed.* 1995; **8**: 387–396.
59. Basser PJ. Inferring microstructural features and the physiological state of tissues from diffusion-weighted images. *NMR Biomed.* 1995; **8**: 333–344.
60. Conturo TE, McKinstry RC, Aronovitz JA, Neil JJ. Diffusion MRI: precision, accuracy and flow effects. *NMR Biomed.* 1995; **8**: 307–332.
61. Le Bihan D. Molecular diffusion, tissue microdynamics and microstructure. *NMR Biomed.* 1995; **8**: 375–386.
62. Nicholson C, Phillips JM. Ion diffusion modified by tortuosity and volume fraction in the extracellular microenvironment of the rat cerebellum. *J. Physiol. (Lond.)* 1981; **321**: 225–257.
63. Sen PN, Scala C, Cohen MH. A self similar model for sedimentary rocks with application to the dielectric constant of fused glass beads. *Geophysics* 1981; **46**: 781–795.
64. Mitra PP, Sen PN, Schwarz LM. Short-time behaviour of the diffusion coefficient as a geometrical probe of porous media. *Phys. Rev. B* 1993; **47**: 8565–8574.
65. Latour LL, Svoboda K, Mitra PP, Sotak CH. Time-Dependent Diffusion of Water in a Biological Model System. *Proc. Natl. Acad. Sci. USA* 1994; **91**: 1229–1233.
66. Latour LL, Mitra PP, Kleinberg RL, Sotak CH. Time-dependent diffusion coefficient of fluids in porous media as a probe of surface-to-volume ratio. *J. Magn. Reson.* 1993; **101A**: 342–346.
67. Szafer A, Zhong J, Gore JC. Theoretical model for water diffusion in tissues. *Magn. Reson. Med.* 1995; **33**: 697–712.
68. Crank J. The Mathematics of Diffusion. Clarendon Press: Oxford, 1975.
69. Stanisz GJ, Szafer A, Wright GA, Henkelman RM. An analytical model of restricted diffusion in bovine optic nerve. *Magn. Reson. Med.* 1997; **37**: 103–111.
70. Tanner JE. Transient diffusion in a system partitioned by permeable barriers. Application to NMR measurements with a pulsed field gradient. *J. Chem. Phys.* 1978; **69**: 1748–1754.
71. Pfeuffer J, Dreher W, Sykova E, Leibfritz D. Water signal attenuation in diffusion-weighted ^{1}H NMR experiments during cerebral ischemia: influence of intracellular restrictions, extracellular tortuosity, and exchange. *Magn. Reson. Imag.* 1998; **16**: 1023–1032.
72. Kärger J, Pfeifer H, Heink W. Principles and application of self-diffusion measurements by nuclear magnetic resonance. *Adv. Magn. Reson.* 1988; **12**: 1–89.
73. Lipinski H-G. Monte Carlo Simulation of extracellular diffusion in brain tissues. *Phys. Med. Biol.* 1990; **35**: 441–447.
74. Ford JC, Hackney DB, Alsop DC, Jara H, Joseph PM, Hand CM, Black P. MRI characterization of diffusion coefficients in a rat spinal cord injury model. *Magn. Reson. Med.* 1994; **31**: 488–494.
75. Ford JC, Hackney DB, Lavi E, Phillips M, Patel U. Dependence of apparent diffusion coefficients on axonal spacing, membrane permeability, and diffusion time in spinal white matter. *J. Magn. Reson. Imag.* 1998; **8**: 775–782.
76. Lehner FK. On the validity of Fick's law for transient diffusion through a porous medium. *Chem. Engng Sci.* 1979; **34**: 821–825.
77. Sykova E, Svoboda J, Polak J, Chvatal A. Extracellular volume fraction and diffusion characteristics during progressive ischemia and terminal anoxia in the spinal chord of the rat. *J. Cereb. Blood Flow Metab.* 1994; **14**: 301–311.
78. Vorisek I, Sykova E. Evaluation of anisotropic diffusion in the developing rat corpus callosum. *J. Neurophysiol.* 1997; **78**: 912–919.
79. van Herreveld A, Dafiny N, Khattab FI. Effects of calcium on electrical resistance and extracellular space of cerebral cortex. *Exp. Neurol.* 1971; **31**: 358–367.
80. Schuier FJ, Hossmann K-A. Experimental brain infarcts in cats. II. Ischemic brain edema. *Stroke* 1980; **11**: 593–601.
81. van Zijl PCM, Moonen CTW, Faustino P, Pekar J, Kaplan O, Cohen JS. Complete separation of intracellular and extracellular information in NMR spectra of perfused cells by diffusion-weighted spectroscopy. *Proc. Natl Acad. Sci.* 1991; **88**: 3228–3232.
82. Flögel U, Niendorf T, Serkova N, Brand A, Henke J, Leibfritz D. Changes in organic solutes, volume, energy state, and metabolism associated with osmotic stress in a glial cell line. *Neurochem. Res.* 1995; **20**: 793–802.
83. Pilatus U, Shim H, Artemov D, Davis D, van Zijl PCM. Intracellular volume and apparent diffusion constants of perfused cancer cell cultures as measured by NMR. *Magn. Reson. Med.* 1997; **37**: 825–832.
84. Pfeuffer J, Flogel U, Leibfritz D. Monitoring of cell volume and water exchange time in perfused cells by diffusion-weighted ^{1}H NMR spectroscopy. *NMR Biomed.* 1998; **11**: 11–18.
85. Mild KH, James TL, Gillen KT. Nuclear magnetic resonance relaxation time and self-diffusion coefficient measurement of water in frog ovarian eggs. *J. Cell. Physiol.* 1972; **80**: 155–158.
86. Trantham EC, Rorschach HE, Clegg JS, Hazlewood CF, Nicklow RM, Wakabayashi N. Diffusive properties of water in artemia cysts as determined from quasi-elastic neutron scattering spectra. *Biophys. J.* 1984; **45**: 927–938.
87. Luby-Phelps K, Castle PE, Taylor DL, Lanni F. Hindered diffusion of inert tracer particles in the cytoplasm of mouse 3T3 cells. *Proc. Natl Acad. Sci. USA* 1987; **84**: 4910–4913.
88. Neil JJ, Duong TQ, Ackerman JJH. Evaluation of intracellular diffusion in normal and globally-ischemic rat brain via ^{133}Cs NMR. *Magn. Reson. Med.* 1996; **35**: 329–335.
89. Duong TQ, Ackerman JJH, Ying HS, Neil JJ. Evaluation of extra-intracellular apparent diffusion in normal and globally ischemic rat brain via ^{19}F NMR. *Magn. Reson. Med.* 1998; **40**: 1–13.
90. Pfeuffer J, Broer S, Broer A, Lechte M, Flogel U, Leibfritz D. Expression of aquaporins in Xenopus laevis oocytes and glial cells as detected by diffusion-weighted ^{1}H NMR spectroscopy and photometric swelling assay. *Biochim. Biophys. Acta* 1998; **1448**: 27–36.
91. Andrasko J. Water diffusion permeability of human erythrocytes studied by a pulsed gradient NMR technique. *Biochim. Biophys. Acta* 1976; **428**: 304–311.
92. Meier C, Dreher W, Leibfritz D. Water diffusion and exchange in rat brain measured in vivo at very high *b*-values. *Proceedings: 7th Meeting of the International Society of Magnetic Resonance in Medicine, Philadelphia*, 1999; 563.
93. Duong TQ, Springer CS, Sotak CH, Bretthorst GL, Vetek G, Palyka I, Ackerman JJH, Neil JJ. Evaluation of equilibrium transcytolemmal water exchange in intact rat brain. *Proceedings: 6th Meeting of the International Society of Magnetic Resonance in Medicine, Sydney*, 1998; 208.
94. Le Bihan D, Turner R, Douek P. Is water diffusion restricted in

human brain white matter? An echo-planar NMR imaging study. *NeuroReport* 1993; **4**: 887–890.
95. van Gelderen P, de Vleeschouwer MHM, DesPres D, Pekar J, van Zijl PCM, Moonen CTW. Water diffusion and acute stroke. *Magn. Reson. Med.* 1994; **31**: 154–163.
96. Horsfield MA, Barker GJ, Ian McDonald W. Self-diffusion in CNS tissue by volume-selective proton NMR. *Magn. Reson. Med.* 1994; **31**: 637–644.
97. Niendorf T, M Dijkhuizen R, Norris DG, van Lookeren Campagne M, Nicolay K. Biexponential diffusion attenuation in various states of brain tissue: implications for diffusion-weighted imaging. *Magn. Reson. Med.* 1996; **36**: 847–857.
98. Kraemer F, Darquie A, Clark CA, le Bihan D. Separation of two diffusion compartments in the human brain. *Proceedings: 7th Meeting of the International Society of Magnetic Resonance in Medicine, Philadelphia*, 1999; 1808.
99. Assaf Y, Cohen Y. Non-mono-exponential attenuation of water and N-acetyl aspartate signals due to diffusion in brain tissue. *J. Magn. Reson.* 1998; **131**: 69–85.
100. Pfeuffer J, Provencher SW, Gruetter R. Water diffusion in rat brain in vivo as detected at very large b values is multi-compartmental. *Magma* 1999; **8**: 98–108.
101. Norris DG, Niendorf T, Hoehn-Berlage M, Kohno K, Schneider EJ, Hainz P, Hropot M, Leibfritz D. The incidence of apparent restricted diffusion in three different models of cerebral infarction. *Magn. Reson. Imag.* 1994; **12**: 1175–1182.
102. Niendorf T, Norris DG, Leibfritz D. Detection of apparent restricted diffusion in healthy rat brain at short diffusion times. *Magn. Reson. Med.* 1994; **32**: 672–677.
103. Norris DG, Niendorf T, Leibfritz D. Healthy and infarcted brain tissues studied at short diffusion times: the origins of apparent restriction and the reduction in apparent diffusion coefficient. *NMR Biomed.* 1994; **7**: 304–310.
104. Kohno K, Back T, Hoehn-Berlage M, Hossmann K-A. A modified rat model of middle cerebral artery thread occlusion under electrophysiological control for magnetic resonance investigations. *Magn. Reson. Imag.* 1995; **13**: 65–71.
105. Davis D, Ulatowski J, Eleff S, Izuta M, Mori S, Shungu D, van Zijl PCM. Rapid monitoring of changes in water diffusion coefficients during reversible ischemia in cat and rat brain. *Magn. Reson. Med.* 1994; **31**: 454–460.
106. Dijkhuizen RM, Berkelbach van der Sprenkel JW, Tulleken CAF, Nicolay K. Correlation between hemodynamics and water diffusion changes in a rat model of acute focal ischemia. *Brain Res.* 1997; **750**: 161–170.
107. Knight RA, Ordidge RJ, Helpern JA, Chopp M, Rodolosi LC, Peck D. Temporal evolution of ischemic damage in rat brain measured by proton nuclear magnetic resonance imaging. *Stroke* 1991; **22**: 802–808.
108. Helpern JA, Dereski MO, Knight RA, Ordidge RJ, Chopp M, Qing ZX. Histopathological correlations of nuclear magnetic resonance imaging parameters in experimental cerebral ischemia. *Magn. Reson. Imag.* 1993; **11**: 241–246.
109. Zhong J, Petroff OAC, Prichard JW, Gore JC. Changes in water diffusion and relaxation properties of rat cerebrum during status epilepticus. *Magn. Reson. Med.* 1993; **30**: 241–246.
110. Benveniste H, Hedlund LW, Johnson GA. Mechanism of detection of acute cerebral ischemia in rats by diffusion-weighted magnetic resonance microscopy. *Stroke* 1992; **23**: 746–754.
111. Hansen AJ, Olsen CE. Brain extracellular space during spreading depression and ischemia. *Acta Physiol. Scand.* 1980; **108**: 355–365.
112. Gardner-Medwin AR, van Bruggen N, Williams SR, Ahier RG. Magnetic resonance imaging of spreading depression in the anaesthetized rat. *J. Cereb. Blood Flow Metab.* 1994; **14**: 7–11.
113. Latour LL, Hasegawa Y, Formato JE, Fisher M, Sotak CH. Spreading waves of decreased diffusion coefficient after cortical stimulation in the rat brain. *Magn. Reson. Med.* 1994; **32**: 189–198.
114. Busch E, Gyngell ML, Eis M, Hoehn-Berlage M, Hossmann K-A. Potassium induced cortical spreading depressions during focal cerebral ischemia in rats: contribution to lesion growth assessed by diffusion-weighted NMR and biochemical imaging. *NMR Biomed.* 1995; **8**: 59–64.
115. Harris NG, Zilkha E, Houseman J, Symms MR, Obrenovitch TP, Williams SR. The relationship between the apparent diffusion coefficient measured by magnetic resonance imaging, anoxic depolarisation, and glutamate efflux during experimental cerebral ischemia. *J. Cereb. Blood Flow Metab.* 2000; **20**: 28–36.
116. Huang NC, Yongbi MN, Helpern JA. The influence of preischemic hyperglycemia on acute changes in brain water ADCw following focal ischemia in rats. *Brain Res.* 1998; **788**: 137–43.
117. Huang NC, Yongbi MN, Helpern JA. The influence of preischemic hyperglycemia on acute changes in the apparent diffusion coefficient of brain water following global ischemia in rats. *Brain Res.* 1997; **757**: 139–45.
118. de Crespigney AJ, Röther J, Beaulieu C, Moseley ME. Correlation of diffusion, blood volume and DC-potential changes in rat brain after cardiac arrest. *Proceedings: 5th Meeting of the International Society of Magnetic Resonance in Medicine, Vancouver*, 1997; 394.
119. der Toorn A van, Sykova E, Dijkhuizen RM, Vorisek I, Vargova L, Skobisova E, Lookeren Campagne M van, Reese T, Nicolay K. Dynamic changes in water ADC, energy metabolism, extracellular space volume, and tortuosity in neonatal rat brain during global ischemia. *Magn. Reson. Med.* 1996; **36**: 52–60.
120. Moseley ME, Cohen Y, Kucharczyk J, Mintorovitch J, Asgari HS, Wendland MF, Tsuruda J, Norman D. Diffusion-weighted MR imaging of anisotropic water diffusion in cat central nervous system. *Radiology* 1990; **176**: 439–445.
121. Conturo TE, Lori NF, Cull TS, Akbudak E, Snyder AZ, Shimony JS, McKinstry RC, Burton H, Raichle ME. Tracking neuronal fiber pathways in the living human brain. *Proc. Natl. Acad. Sci. USA* 1999; **96**: 10422–10427.
122. Mori S, Crain BJ, Chacko VP, van Zijl PCM. Three-dimensional tracking of axonal projections in the brain by magnetic resonance imaging. *Ann. Neurol.* 1999; **45**: 265–269.
123. Beaulieu C, Allen PS. Determinants of anisotropic water diffusion in nerves. *Magn. Reson. Med.* 1994; **31**: 394–400.
124. Beaulieu C, Allen PS. Water diffusion in the giant axon of the squid: implications for diffusion-weighted MRI of the nervous system. *Magn. Reson. Med.* 1994; **32**: 579–583.
125. Beaulieu C, Fenrich FR, Allen PS. Multicomponent water proton transverse relaxation and T_2-discriminated water diffusion in myelinated and nonmyelinated nerve. *Magn. Reson. Imag.* 1998; **16**: 1201–1210.
126. Wimberger DM, Roberts TP, Berkovich AJ, Prayer LM, Moseley ME, Kucharczyk J. Identification of "premyelination" by diffusion-weighted MRI. *J. Comput. Assist. Tomogr.* 1995; **19**: 28–33.
127. Ono J, Harada K, Takahashi M, Maeda M, Ikenaka K, Sakurai K, Sakai N, Kagawa T, Fritz-Zieroth B, Nagai T, Nihei A, Hashimoto S, Okada S. Differentiation between dysmyelination and demyelination using magnetic resonance diffusional anisotropy. *Brain Res.* 1995; **671**: 141–148.
128. Hüppi PS, Maier SE, Peled S, Zientara GP, Barnes PD, Jolesz FA, Volpe JJ. Microstructural development of human newborn cerebral white matter assessed by diffusion tensor magnetic resonance imaging. *Pediatr. Res.* 1998; **44**: 584–590.
129. Neil JJ, Shiran SI, Mckinstry RC, Schefft GL, Snyder AZ, Almli CR, Akbudak E, Aronovitz JA, Miller JP, Lee BCP, Conturo TE. Normal brain in human newborns—apparent diffusion coefficient and diffusion anisotropy measured by using diffusion tensor MR imaging. *Radiology* 1998; **209**: 57–66.
130. Baratti C, Barnett AS, Pierpaoli C. Comparative MR imaging study of brain maturation in kittens with T_1, T_2, and the trace of the diffusion tensor. *Radiology* 1999; **210**: 133–142.
131. Moseley ME, Mintorovitch J, Asgari H, Vexler Z, Kucharczyk J. Diffusion/perfusion MR characterization of hyperacute cerebral ischemia. *Proceedings: 10th Meeting of the Society of Magnetic Resonance in Medicine, San Francisco*, 1991; 330.
132. Helpern JA, Ordidge RJ, Knight RA. The effect of cell membrane water permeability on the apparent diffusion coefficient of water. *Proceedings: 11th Annual Meeting of the Society of Magnetic Resonance in Medicine, Berlin*, 1992; 1201.
133. Pfeuffer J, Flogel U, Dreher W, Leibfritz D. Restricted diffusion and exchange of intracellular water: theoretical modelling and diffusion time dependence of ^{1}H NMR measurements on perfused glial cells. *NMR Biomed.* 1998; **11**: 19–31.

134. der Toorn A van, Verheul HB, der Sprenkel JW van, Tulleken CA, Nicolay K. Changes in metabolites and tissue water status after focal ischemia in cat brain assessed with localized proton MR spectroscopy. *Magn. Reson. Med.* 1994; **32**: 685–691.
135. Wick M, Nagatomo Y, Prielmeier F, Frahm J. Alteration of intracellular metabolite diffusion in rat brain in vivo during ischemia and reperfusion. *Stroke* 1995; **26**: 1930–1933.
136. der Toorn A van, Dijkhuizen RM, Tulleken CA, Nicolay K. Diffusion of metabolites in normal and ischemic rat brain measured by localized ^{1}H MRS. *Magn. Reson. Med.* 1996; **36**: 914–922.
137. Szafer A, Zhong J, Anderson AW, Gore JC. Diffusion-weighted imaging in tissues: theoretical models. *NMR Biomed.* 1995; **8**: 289–296.